Computers and Concrete, *Vol. 17, No. 3 (2016) 305-322*
DOI: http://dx.doi.org/10.12989/cac.2016.17.3.305

Assessment of design methods for punching through numerical experiments

Gregoria M. Kotsovou[*1], Gerasimos M. Kotsovos[2a] and Emmanuel Vougioukas[3b]

[1]*Heriot Watt University, Edinburgh, U.K.*
[2]*Lithos Consulting Engineers, Vari, Greece*
[3]*National Technical University of Athens, Athens, Greece*

(Received December 12, 2015, Revised February 17, 2016, Accepted February 18, 2016)

Abstract. The work is intended to demonstrate that the loss of bond between concrete and flexural steel which led in recent years a number of flat-slab structures to punching collapse under service loading conditions is also relevant to ultimate limit-state design. It is based on a comparative study of the results obtained from numerical experiments on flat slab-column sub-assemblages. The slabs were designed for punching either in compliance with the EC2 code requirements, which do not allow for such loss of bond, or in accordance with the compressive force-path method which considers the loss of bond between concrete and the flexural reinforcement in tension as the primary cause of punching. The numerical experiments are carried out through the use of a nonlinear finite element analysis package for which, although ample published evidence of its validity exists, additional proof of its suitability for the purposes of the present work is presented.

Keywords: compressive force path method; design of concrete structures; numerical experiments; flat slabs; punching

1. Introduction

The collapse of flat-slab structures in recent years (New Civil Engineer 1997, Aoude *et al.* 2013) has caused concerns regarding the ability of current design practice to safeguard an adequate margin of safety against punching. The investigation of the causes of these collapses revealed that punching occurred due to the loss of bond between concrete and the flexural tension reinforcement of the flat slab in the region of its intersection with the supporting column (Kellermann 1997); loss of bond occurred under service loading conditions as a result of the use of de-icing salts. However, it should be expected that yielding of the flexural reinforcement may also lead to de-bonding of the steel from concrete, and, although this has been considered as one of the causes of brittle failure (Kotsovos 2014), punching included (Kotsovos and Kotsovos 2009, Kotsovos and Kotsovos 2010), it has not as yet been allowed for by the methods adopted by current codes of practice for

*Corrsesponding author, Ph.D., E-mail: G.Kotsovou@hw.ac.uk
[a]Ph.D., E-mail: gkotsov@gmail.com
[b]Ph.D., E-mail: manolis@central.ntua,gr

http://www.techno-press.org/?journal=cac&subpage=8 ISSN: 1598-8198 (Print), 1598-818X (Online)

the design of concrete structures (e.g., Eurocode 2 2004, Mosley *et al*. 2012).

To this end, the aim of the present work is to investigate by means of numerical experiments the ability of the design method adopted by EC2 for safeguarding against punching. For purposes of comparison, an alternative design method – the compressive force path (CFP) method – is also investigated, since the latter method allows for the effect of the loss of bond between concrete and steel on punching. The numerical experiments are carried out through the use of a nonlinear (NL) finite element analysis (FEA) package which is fully described elsewhere (Kotsovos and Pavlovic 1995, ADINA 2012, Kotsovos 2015) and has been shown to produce realistic predictions of structural concrete behaviour in all cases investigated to date. Further evidence of the package's validity is provided herein through a comparison of the package's predictions with values of load-carrying capacity obtained from physical tests carried out by Yamada *et al*. (1992) on flat slabs. Similar slabs differing only as regards the amount and arrangement of the transverse reinforcement, the latter designed in accordance with the EC2 and CFP methods, are used for investigating the ability of these methods to safeguard against punching.

2. Design methods for puncing

The methods of design assessed herein are outlined in what follows by reference to Figs. 1 and 2. Fig. 1 shows the portion of a slab supported by a rectangular grid of columns. The figure also provides a schematic representation of the bending moment diagrams of the slab under transverse loading. The portion of the slab enclosed by the geometric locus of the points of zero bending moment around the central slab support is shown in isolation in Fig. 2, where the geometric locus of zero bending moment is marked with "3". For the rectangular slab indicated in the latter figure, curve "3" may have an elliptical shape, which, however, may become circular for a square slab. Punching is usually investigated by testing rectangular slab-column sub-assemblages, such as that shown in Fig. 2, supported at the lower-column end and subjected to symmetrical loading at locations considered to lie on the geometric locus of zero bending moment encompassing the supporting column. Such structural elements have formed the subject of numerous experimental investigations carried out to date (e.g., Task Group 3.1/4.10 2001, Kinnunen *et al*. 2001, Oliveira *et al*. 2004, Papanikolaou *et al*. 2005, Hegger *et al*. 2006, Mutoni 2008, Birkle and Dilger 2008).

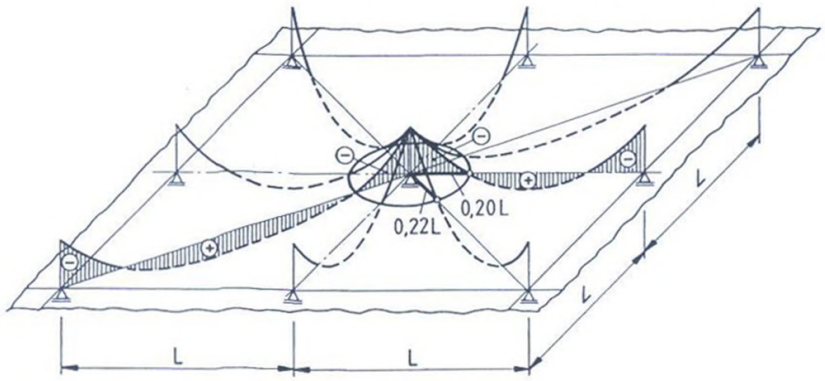

Fig. 1 Schematic representation of distribution of bending moment developing in a flat slab under transverse load

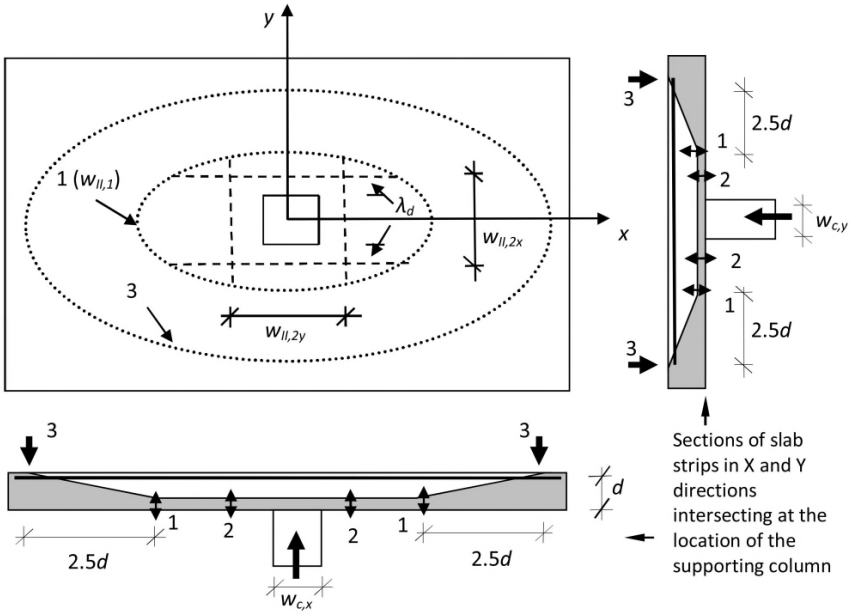

Fig. 2 Schematic representation of the physical state of a rectangular slab (considered to model the portion of the flat slab (in Fig. 1) encompassed by the geometric locus of zero bending moment (curve3)) indicating locations 1 and 2 of possible punching initiation in accordance with the CFP method

2.1 CFP method

The CFP method might appear, at first sight, to be a rather unorthodox way of designing structural concrete. However, it is easy, with hindsight, to see that it conforms largely to the classical design of masonry structures by Greek and Roman Engineers. These tended to rely greatly on arch action-later expressed (and extended) through the Byzantine dome and the Gothic vaulting. Now, such a mechanism of load transfer may seem largely irrelevant for a beam exhibiting an elastic response. However, for a cracked reinforced concrete girder close to failure the parallel with an arch-and-tie system reveals striking similarities between the time-honoured concept of a compressive arch and the CFP method.

The method, which is fully described in Kotsovos 2014, has been developed within the context of the limit-state philosophy and involves, on the one hand, the identification of the regions of a structural member or structure at its ultimate limit state through which the external load is transmitted from its point of application to the supports, and, on the other hand, the strengthening of these regions so as to impart to the member or structure desired values of load-carrying capacity and ductility. As most of the above regions enclose the trajectories of internal compressive actions, the method has been termed the ‘compressive-force path’ (CFP) method. In contrast to the methods implemented in current codes of practice, the CFP method is fully compatible with the behaviour of concrete (as described by valid experimental information) at both the material and structure levels and capable of producing design solutions that have been found to satisfy the code performance requirements in all cases investigated to date.

As for the case of most methods adopted to date for the design of structural concrete, the

implementation of the CFP method to punching is essentially an extension of the manner in which it is used for the design of beam/column elements. In accordance with the method, punching is considered likely to initiate at either of the following locations:

(a) Along a curve, marked as "1" in Fig. 2, similar in shape with curve "3", with the distance (in the radial direction) between curves "1" and "3" being equal to 2.5d, where d is the slab effective depth. Assuming that curve "1" is a circle, the punching capacity of the slab is obtained by

$$P_{II,1} = 0.5\, f_t\, \pi\, Dd \tag{1}$$

where D is the radius of curve "1" and f_t the tensile strength of concrete.

If $P_{II,1}<P_d$, where P_d is the design value of the punching load, then reinforcement in the form links is uniformly distributed within the circular strip extending between the circles with radii $D/2-d$ and $D/2+d$ in an amount sufficient to sustain the whole punching load (i.e., the contribution of concrete to resisting punching is considered to be negligible and, therefore, neglected).

(b) Within the portion of the slab strips intersecting at the location of the supporting column and extending in the direction of the flexural reinforcement to the strip-curve "1" intersections. In this case, the punching capacity is obtained by

$$P_{II,2} = 4V_{II,2} = 4\, F_c[1-1/(1+5|f_t|/f_c)] \tag{2}$$

where $V_{II,2}$ is the shear capacity of each of the four slab strips on each side of the supporting column, F_c the force sustained by the compressive zone of each of the slab strips on account of bending, and f_t, f_c the values of the uniaxial tensile and compressive strength of concrete, respectively. The slab strips extend to a distance of λd on either side of the supporting column (see Fig. 2), i.e., the strip width is

$$w_{II,2} = w_c + 2\lambda d \tag{3}$$

where w_c is the column width along the axes of symmetry (x or y); d, the effective depth of the slab; and λ, a parameter describing the effect of (i) concrete strength (f_c) and (ii) the ratio (ρ) and yield stress (f_y) of the flexural reinforcement in tension, expressed as

$$\lambda = \lambda_1\lambda_2 = (2-100\,\rho\, f_y/500)[1+0.01(f_c-60)] \tag{4}$$

with λ_1 and λ_2 being always not smaller than 1.

As for the case **(a)**, if $P_{II,2}<P_d$, then reinforcement in the form of vertical and horizontal bars is uniformly distributed within the aforementioned portion of the slab strips in an amount sufficient to sustain the whole punching load (i.e., the contribution of concrete to resisting punching is considered to be negligible). The amount of reinforcement required per unit length in this case is obtained by

$$A_{sv,II2v} = T_{II,2v}/f_{yv} \text{ (vertical)};\ A_{sv,II2h} = T_{II,2h}/f_{yv} \text{ (horizontal)} \tag{5}$$

where $T_{II,2v} = \sigma_t\, w_{II,2}/2$, $T_{II,2h} = \sigma_t x/2$, and $\sigma_t = f_c/[5(F_c/V_d-1)]$ with x being the depth of the compressive zone of the slab strip and V_d the design value of the shear force of a slab strip.

2.2 EC2 method

As for the case of the CFP method, the method adopted by EC2 for punching is an extension of the method adopted for shear design which is based on the use of truss or strut-and-tie models initially proposed by Ritter (1899) and Morsch (1902). The punching shear stress sustained by the

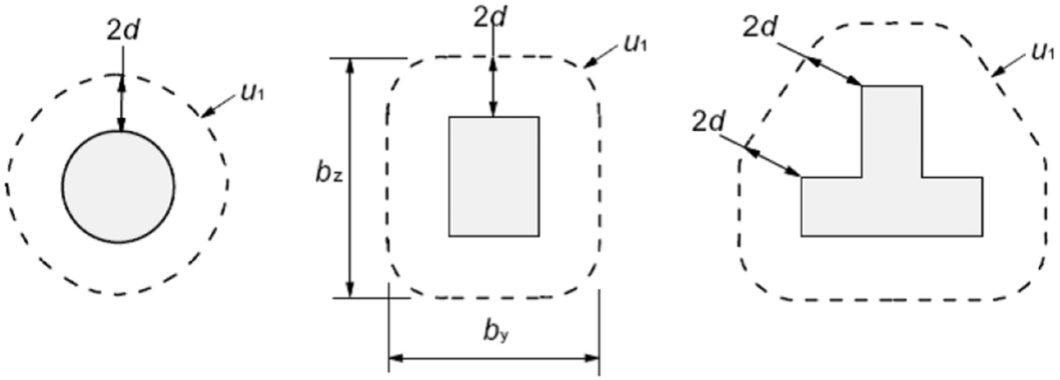

Fig. 3 Basic control perimeter in accordance with EC2

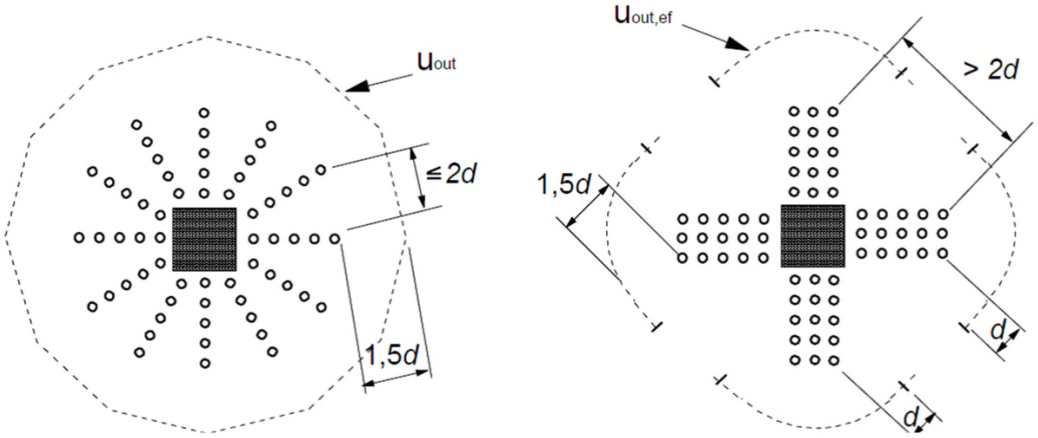

Fig. 4 Arrangements of punching reinforcement in accordance with EC2

slab without the contribution of reinforcement for punching is given by

$$v_{Rd} = C_{Rd,c}k(100\rho_l f_{ck})^{(1/3)} < v_{Rd,max} \tag{6}$$

where ρ_l is the flexural tensile reinforcement ratio, f_{ck} the characteristic uniaxial compressive strength of concrete, $k = 1 + (200/d)^{0.5}$ (but not larger than 2), and $C_{Rd,c} = 0.18$. The first check for punching failure is carried out at the "basic control perimeter u_1" taken at a distance $2d$ from the supporting column and constructed such as its length is minimised (see Fig. 3). If $v_{Rd} < v_{Ed}$, where v_{Ed} is the design shear stress, then reinforcement is required. The total reinforcement required to prevent punching within the area enclosed by the control perimeter is calculated from

$$A_{sv} = (V_{Ed} - 0.75V_{Rd,c})/f_{y,red} \tag{7}$$

where $f_{y,red} = 250 + 0.25d \leq f_{yvd}$, d in mm, f_{yvd} the design yield stress of the shear reinforcement, V_{Ed} the design value of punching shear and $V_{Rd,c}$ the punching capacity of the slab without transverse reinforcement. It should be noted that such reinforcement extends to a distance of $1.5d$ from the edge of the supporting column and it can be arranged as indicated in Fig. 4. The checks for punching continue by increasing the distance of the control perimeter until $v_{Rd} > v_{Ed.}$

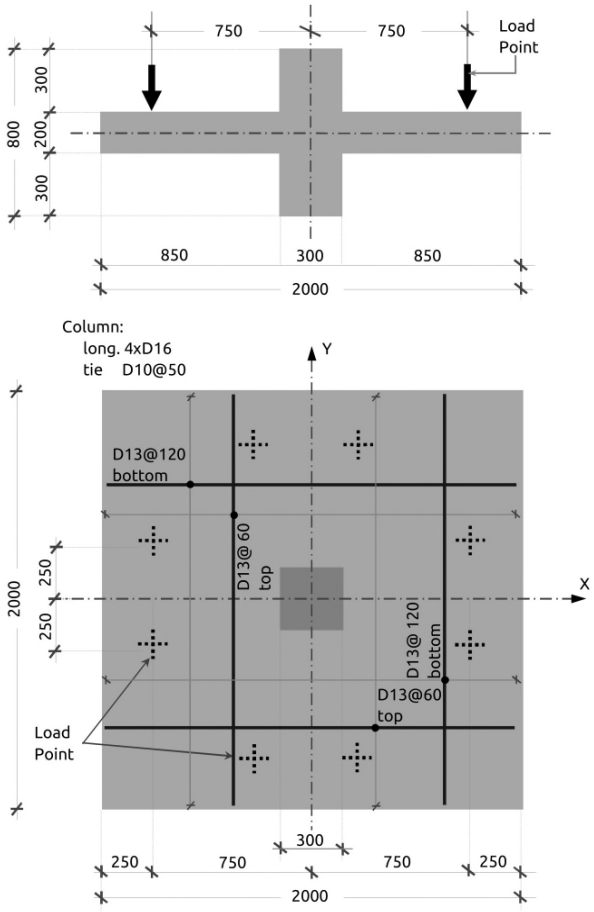

Fig. 5 Geometric characteristics and flexural reinforcement details of a typical slab-column sub-assemblage investigated: (top) elevation; (bottom) plan

3. Numerical experiments

3.1 Structural forms investigated

The structural forms investigated in the present work are slab-column sub-assemblages similar to those denoted as T1, T5, K1 and K7 in Yamada *et al*. (1993), where full details of these specimens are provided; therefore, only the information relative to the present work is outlined in what follows. The elevation and plan of a typical specimen is shown in Fig. 5. The slab is square with a 2000 mm side and a centrally located column with a square 300 mm side cross section. The column extends above and below the slab for a length of 300 mm. The specimen is supported by the lower-column stud resting directly on the laboratory floor. The longitudinal reinforcement is symmetrically distributed in the orthogonal *X* and *Y* directions with minimum clear cover of 20 mm at both the top and bottom slab faces. For all specimens and for both top and bottom faces, bars in the *X* direction are placed directly above bars in the *Y* direction. This flexural reinforcement arrangement provides identical clearance in the two orthogonal directions.

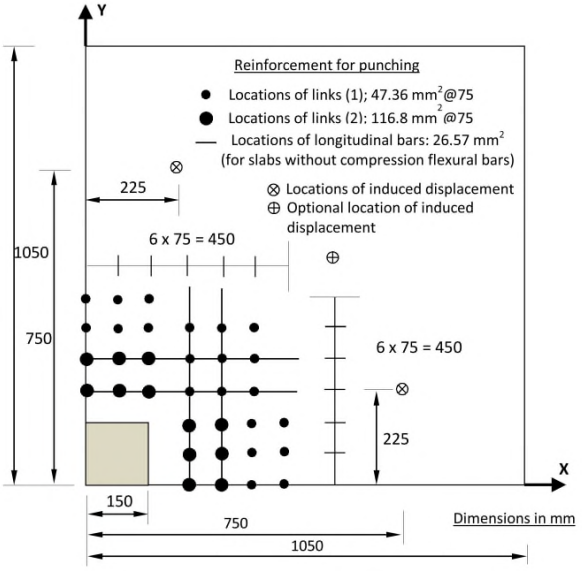

Fig. 6 Reinforcement details for punching in accordance with the CFP method

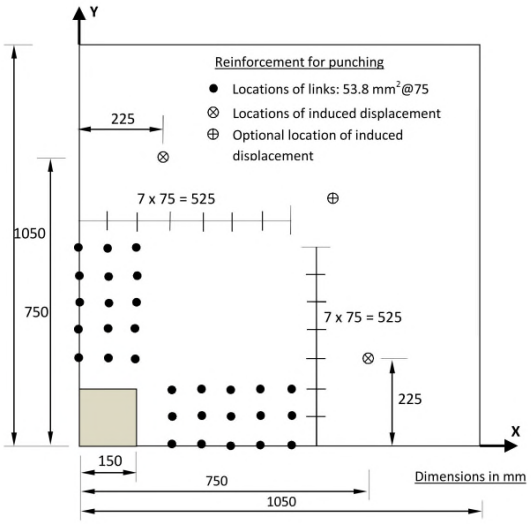

Fig. **7** Strip reinforcment for punching specified by EC2

Specimens T1 and T5 differ from specimens K1 and K6 only in the amount of the longitudinal reinforcement and the amount and arrangement of the transverse reinforcement. In the *T* specimens, the longitudinal reinforcement comprises twenty nine 13 mm diameter bars at 60 mm spacing in the tensile zone (reinforcement ratio ρ_t=1.23%) and fifteen 13 mm diameter bars at 120 mm spacing in the compressive zone (reinforcement ratio ρ_c=0.60%) with a yield stress f_y=800 MPa. In the *K* specimens, the longitudinal reinforcement comprises twenty three 16 mm diameter bars at 80 mm spacing in both the compressive and tensile zones (reinforcement ratios ρ_t=ρ_c=1.53%) with a yield stress f_y=568 MPa. In all specimens, the column reinforcement consists

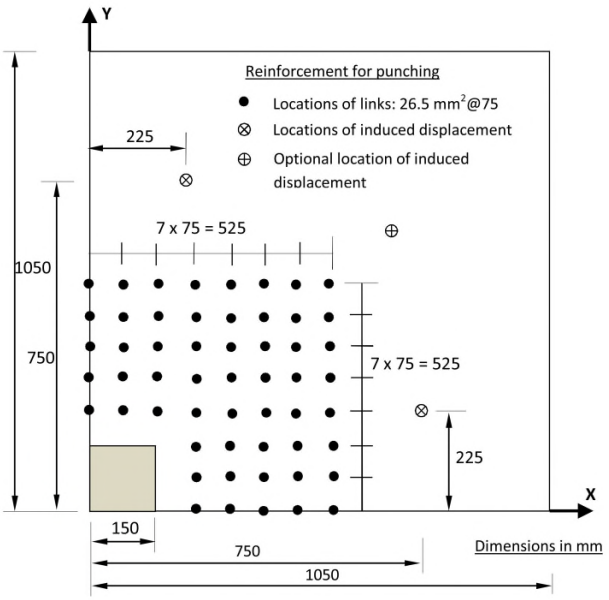

Fig. 8 Uniformly-distributed reinforcment for punching specified by EC2

of four 16 mm diameter corner bars with a yield stress f_y=568 MPa and 10 mm diameter stirrups with a yield stress f_y=360 MPa at 50 mm spacing.

Specimens T1 and K1 are not reinforced for punching. For specimen T5, the transverse reinforcement comprises two 16 mm diameter two-legged stirrups with a yield stress f_y=360 MPa. The stirrups are placed within slab strips along the *X* and *Y* axes of symmetry of the slab at 100 mm spacing across and 130 mm spacing along the strips. For specimen K6, the transverse reinforcement comprises 13 mm diameter links with a yield stress f_y=330 MPa placed at the intersection of the longitudinal bars (i.e., at a spacing of 80 mm in both *X* and *Y* directions). The uniaxial cylinder compressive strength of concrete (f_c) at the time of testing is 21 MPa and 24 MPa for specimens T1 and T5, and 26 MPa and 28 MPa for specimens K1 and K6, respectively.

Monotonic static load is applied downwards at eight points symmetrically distributed round the column centre as indicated in Fig. 5. The lower column stud acts as the reaction support (see Fig. 5). The load applied by two hydraulic jacks connected to the same pump is deflection controlled.

In the present work, further evidence of the validity of the NLFEA package adopted for carrying out the numerical experiments is first obtained through a comparison of the numerically predicted structural behaviour with its experimentally established counterpart for both T1 and T5 and K1 and K6 specimens, and then the package is used to investigate slab-column specimens similar to those of the physical tests in all respects except for the reinforcement which, for the purposes of the present work, is designed in accordance with the methods described in Section 2. The specimens are designated by adopting a two-part name, with the first part (*T* or *K*) denoting specimen details (geometry and flexural reinforcement) relevant to either the *T* or the *K* specimens and the second part the method adopted for designing the reinforcement safeguarding against punching: CFP when the reinforcement is designed in accordance with the CFP method and EC2S or EC2U when the reinforcement is designed in accordance with EC2 and distributed either within strips along the *X* and *Y* axes of symmetry of, or uniformly distributed within, the slab.

As discussed earlier, for the *T*-specimens $\rho_C=0.5\rho_T$, whereas for the *K*-specimens $\rho_C=\rho_T$. In order to investigate the effect of the compression flexural reinforcement on punching the numerical testing is complemented with the testing of an additional set of K-specimens with $\rho_C=0$. The reinforcement for punching designed so as to safeguard a load-carrying capacity of 1500 kN is indicated in Figs. 6 to 8. It is interesting to note in the figures that the resulting reinforcement does not differ only in the amount and arrangement of the transverse reinforcement specified by each of the methods adopted, but, also in that the CFP method also specifies horizontal reinforcement within the compressive zone of the slab in the region of the supporting column for the case of the specimens with $\rho_C=0$.

The comparative study of the CFP method and EC2 provisions is complemented by considering the case of imposing displacement controlled load not only at the points shown in Figs. 6-8, but also at points of the diagonal axes of symmetry of the slab lying on the perimeter formed by the original load points (see Figs. 6-8). Finally, the case is considered of designing reinforcement for punching at a load of 760 kN for the reasons discussed in section 5.2.

3.2 FE model

As discussed in Section 1, the behaviour of the structural forms investigated is established from the results obtained from numerical experiments carried out through the use of a FE package which has been found to produce realistic predictions of structural-concrete behaviour in all cases investigated to date. Full details of the package may be found in numerous publications which formed the subject of two textbooks (Kotsovos and Pavlovic 1995, Kotsovos 2015) and in the manual of the well-known package ADINA (2012) where the model has been recently incorporated.

The package is capable of performing not only static, but also dynamic analysis, the latter being effected through the unconditionally stable average acceleration method of the implicit Newmark integration scheme. Moreover, it uses three-dimensional (3D) non-linear (NL) analysis in order to allow for (a) the NL behaviour of concrete under triaxial stress conditions, which invariably develop prior to local failure (i.e., cracking), and (b) the introduction of non-homogeneity and stress redistribution after the occurrence of cracking. Concrete is modelled by using 27-node brick Lagrangian elements, whereas 3-node isoparametric line elements of appropriate cross-sectional area possessing axial stiffness only are used to model the steel reinforcement.

The nonlinear analysis is based on the iterative procedure known as the modified Newton-Raphson which is used to calculate stresses, strains and residual forces. Every Gauss point is checked, at first, in order to determine whether loading or unloading takes place, and then in order to establish whether any cracks close or form. The development of a crack is followed by immediate loss of load-carrying capacity in the direction normal to the plane of the crack. At the same time, shear stiffness is also reduced drastically to 10% of its value before the occurrence of the crack. Three cracks can form at each integration point, with the first crack modifying the state of stress from triaxial to biaxial, the second, from biaxial to uniaxial, and the third leading to local loss of load-carrying capacity.

Depending on the results of the previous checks, changes are introduced to the stress-strain matrices of the individual FE's and, consequently, to the stiffness matrix of the structure. Based on these modified matrices, deformation, strain and stress corrections are evaluated. Convergence is accomplished once the above corrections become very small. It should be pointed out that the formation and closure of cracking is checked separately during each load step.

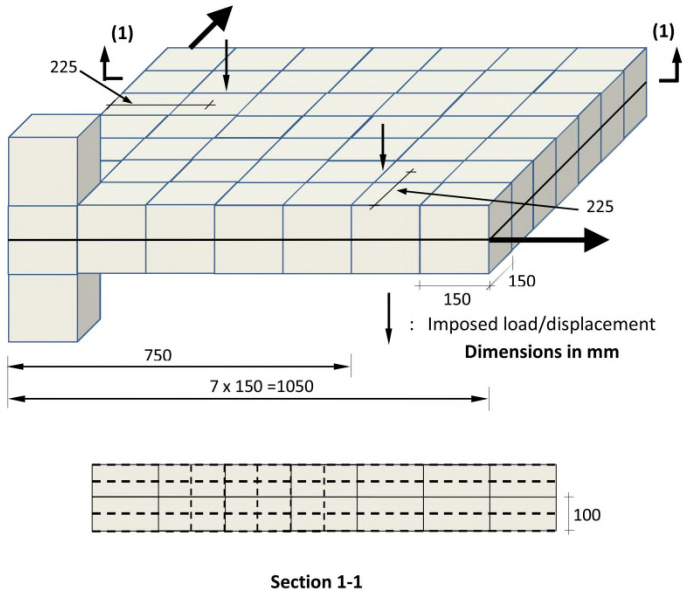

Fig. 9 FE discretization of slab-column sub-assemblage investigated

The implementation of the above procedure is based on the use of suitable analytical models describing the behaviour of concrete, steel and their interaction under short-term loading conditions. Although the models adopted for this purpose are fully described in Kotsovos and Pavlovic (1995), it is important to highlight some of their main features. The material model of concrete behaviour is characterised by both simplicity (fully brittle, with neither strain-rate nor load-path dependency, fully defined by a single material parameter − the uniaxial cylinder compressive strength f_c) − and attention to the actual physical behaviour of concrete in a structure (unavoidable triaxiality which is described on the basis of experimental data of concrete cylinders under definable boundary conditions).

The material model used to describe the deformational behaviour of the steel reinforcement in either tension or compression follows current code recommendations, so that the stress-strain curve is fully defined by using the values of the yield stress and the ultimate strength together with the values of the corresponding strains, with the yield strain taken as the ratio of the yield stress to the elastic modulus of elasticity. Finally, the assumption of perfect bond is considered to provide an adequate description of the interaction between steel and concrete. This is compatible with the smeared-crack approach adopted for the analytical description of the cracking processes of concrete, as well as the fact that the tensile strength of concrete is smaller than that of the experimentally-established strength of the bond between the two materials.

The FE model of the slab-column sub-assemblage shown in Fig. 5 is depicted in Fig. 9, which, due to the two-fold symmetry of the structure, shows only one quarter of the sub-assemblage. From the figure, it can be seen that the slab is subdivided into 7×7×2 27-node Lagrangian 150 mm ×150 mm×100 mm brick concrete elements; such elements are also used for modelling concrete in the column (1×1×2 elements for the part common to the slab and the column and 1×1×1 elements for the column extension both above and below the slab). The reinforcement bars are represented

by 3-node line elements aligned between successive brick-element nodes in both the vertical and horizontal directions as depicted by the dashed lines in section 1-1 included in the figure. Both the flexural and the punching reinforcement arrangement is equivalent to that of the specimens investigated in terms of both bar location and cross-sectional characteristics.

It is important to note that the size of the 27-node Lagrangian brick finite elements (FEs) used is dictated by the philosophy upon which the FE model adopted for the present work, which does not employ small FEs. This is because the material model incorporated in the FE model is based on data obtained from experiments in which concrete cylinders were subjected to various triaxial loading conditions. Consequently these cylinders are considered to constitute a 'material unit' for which average material properties are obtained and hence the volume of these specimens provides a guideline to the order-of-magnitude of the size of the FE used for the modelling of concrete structures (Kotsovos and Pavlovic 1995).

4. Results

The main results obtained from the numerical experiments are shown in Figs. 10 to 13 and Tables 1 to 4. Figs. 10 and 11 show typical load-deflection curves of the slabs investigated, with Fig. 10 describing the effect of the design methods assessed on the load-deflection curves with ρ_C=ρ_T, whereas Fig. 11 depicts the effect of varying ρ_C on the slabs designed in accordance with the CFP method. Figs. 12 and 13 depict typical numerically-established crack patterns of the slabs at various stages of the applied load. Finally, the numerically-obtained values of load-carrying of all slabs investigated are presented in Tables 1 to 4 and used as the basis for a comparative study of the parameters investigated.

5. Discussion of results

5.1 Verification of numerical tool

From Table 1, it can be seen that the NLFEA package used for carrying-out the numerical experiments produces values of load-carrying capacity which deviate from their counterparts established from physical tests less than 13%. More specifically, for the specimens with only flexural reinforcement, the deviation of the predicted values is on average 3%; load-carrying capacity is overestimated by 4%, for specimen T1, and underestimated by 9%, for specimen K1. As regards the specimens with both flexural reinforcement and reinforcement across the slab depth, the deviation of the predicted values are on average 12%; for both specimens load-carrying capacity is underestimated, 11% for specimen T5 and 13% for specimen K7. Since the validity of the methods of design is investigated on the basis of the behaviour of specimens with both flexural reinforcement and steel bars across the slab depth, it is assumed that a numerically calculated value of load-carrying capacity of the order of 12% smaller than the un-factored design value is a sufficiently accurate estimate of the latter.

5.2 Numerical assessment of design methods

From Table 2, it can be seen that the numerically obtained values of load-carrying capacity for

Table 1 Comparison of values of load-carrying capacity obtained from numerical and physical experiments

specimen	punching reinforcement	experimental load-carrying capacity - kN		numerical/ physical
		physical	numerical	
T1	without	441	460	1,04
K1		658	599	0,91
mean value				**0,97**
T5	with	762	680	0,89
K7		1498	1302	0,87
mean value				**0,88**

Table 2 Variation of load-carrying capacity of the specimens tested for various amounts of compression flexural reinforcement with the method of design

specimen	ρ_C/ρ_T	load-carrying capacity - kN		FEA/ des	EC2/ CFP	EC2-u/ EC2-s
		design	FEA			
K-CFP	0	1500	1301	0.87	-	-
K-EC2s			1008	0.67	0.77	-
K-EC2u			990	0.66	0.76	0.99
T-CFP	0.5		1318	0.88	-	-
T-EC2s			1039	0.69	0.78	-
T-EC2u			941	0.63	0.72	0.92
K-CFP	1		1290	0.86	-	-
K-EC2s			1100	0.73	0.85	-
K-EC2u			881	0.59	0.69	0.81

the specimens designed in accordance with the CFP method (see Fig. 6) is smaller than the intended target value by an amount of the order of 12%. Such an underestimate is similar to that of the numerically obtained values of load-carrying capacity of specimens T5 and K7 from their counterparts established from physical test (see Table 1). As discussed in the preceding section, numerically-obtained values exhibiting such a deviation from their assumed "true" counterparts are considered to provide a sufficiently accurate indication of the specimen's load-carrying capacity, and, on such a basis, Table 2 indicates that designing the specimens in accordance with the CFP method achieves the design aim for load-carrying capacity independently of the value of ρ_c which, as discussed in section 3.1, were considered in the present work (see also Fig. 11).

On the other hand, the table indicates that the load-carrying capacity of the specimens designed in accordance with EC2 (see Figs. 7 and 8), in all cases, is smaller than that of their counterparts designed in accordance with the CFP method by an amount which varies between 20% and 30%. This difference in load-carrying capacity is also indicated by the load-deflection curves shown in Fig. 10, which also shows that the method of design does not have any significant effect on the specimen stiffness, the latter being essentially controlled by the flexural characteristics.

The reason for such difference in behaviour reflects the fact that the method of design adopted by EC2 does not recognize that one of the main causes of punching is the development of tensile stresses across both the depth and width of the compressive zone of the slab strips along the *X* and

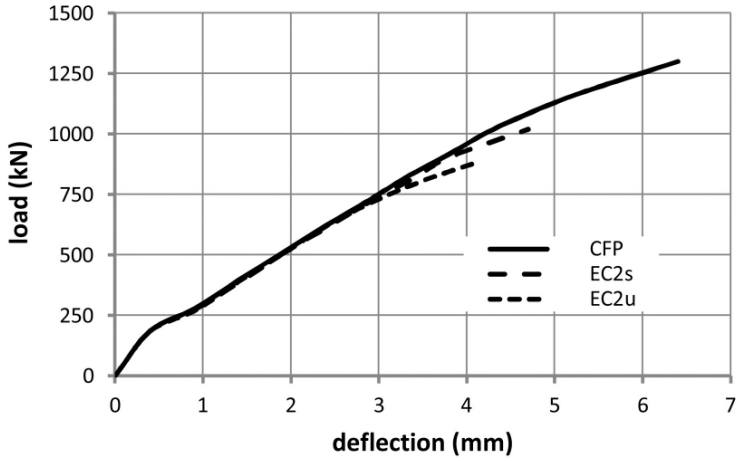

Fig. 10 Effect of design method on the load-deflection curves of slabs with $\rho_C = \rho_T$

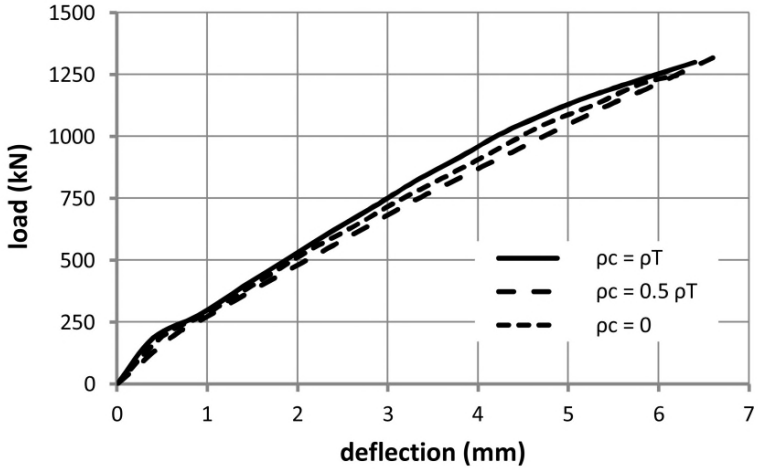

Fig. 11 Effect of ρ_C on the load-deflection curves of slabs designed in accordance with the CFP method

Y axes of symmetry of the slab in the region of their intersection with the supporting column; the development of such stresses occurs due to yielding of the flexural tension reinforcement (Kotsovos 2014). In fact, loss of load-carrying capacity of the specimens designed in compliance with the EC2 requirements occurs when the flexural tension reinforcement yields in the region of the slab-column intersection. On the other hand, such yielding is insufficient to cause loss of load-carrying capacity of the specimens designed in accordance with the CFP method; loss of load-carrying capacity of the latter specimens occurs after yielding of the flexural tension reinforcement bars around the supporting column.

It is interesting to note in Figs. 12 and 13 that, just before and when the maximum sustained load is attained, the crack patterns of the specimens are characterised by the occurrence of both horizontal and vertical cracking within the compressive zone of the slab in the region of the supporting column. The occurrence of such cracking confirms the significance of the transverse

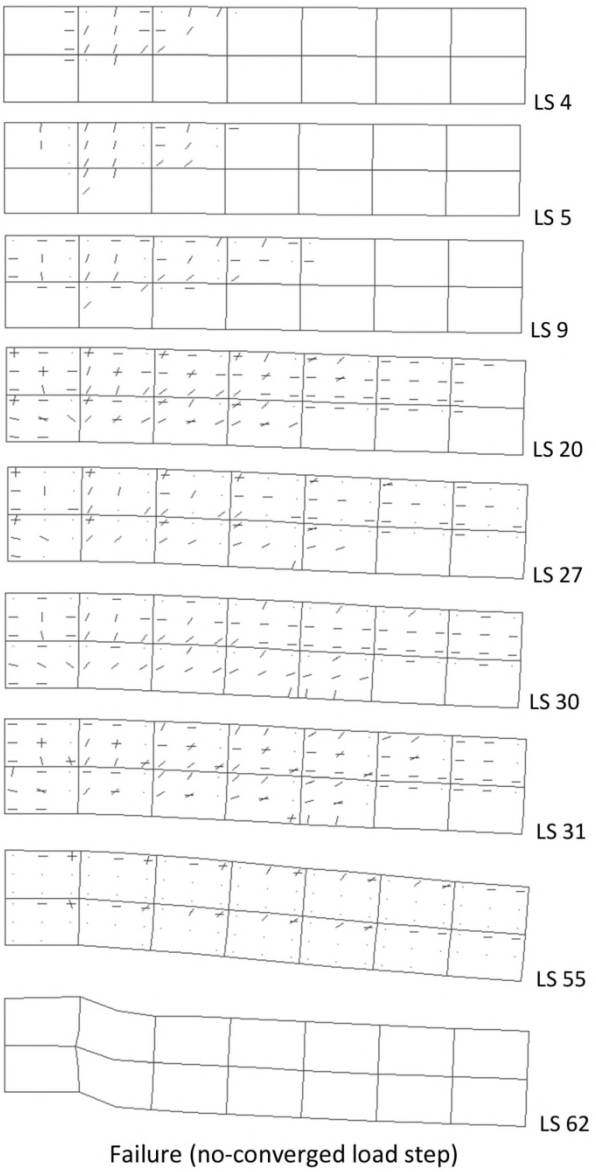

Fig. 12 Typical crack patterns at various load steps (LS) of the slabs designed in accordance with the CFP method

tensile stresses developing within the compressive zone after yielding of the tensile flexural reinforcement for design purposes. The figures also show that, as the load increases, more than one cracks form at particular locations: two intersecting dashes represent the occurrence of two cracks at the same location, whereas a dot indicates local loss of load-carrying capacity due to the occurrence of a third crack at the same location. The last plots at LS 62 in Fig. 11 and at LS 60 in Fig. 12 depict only the deformed shape of the slab at the moment the analysis was interrupted due to lack of convergence.

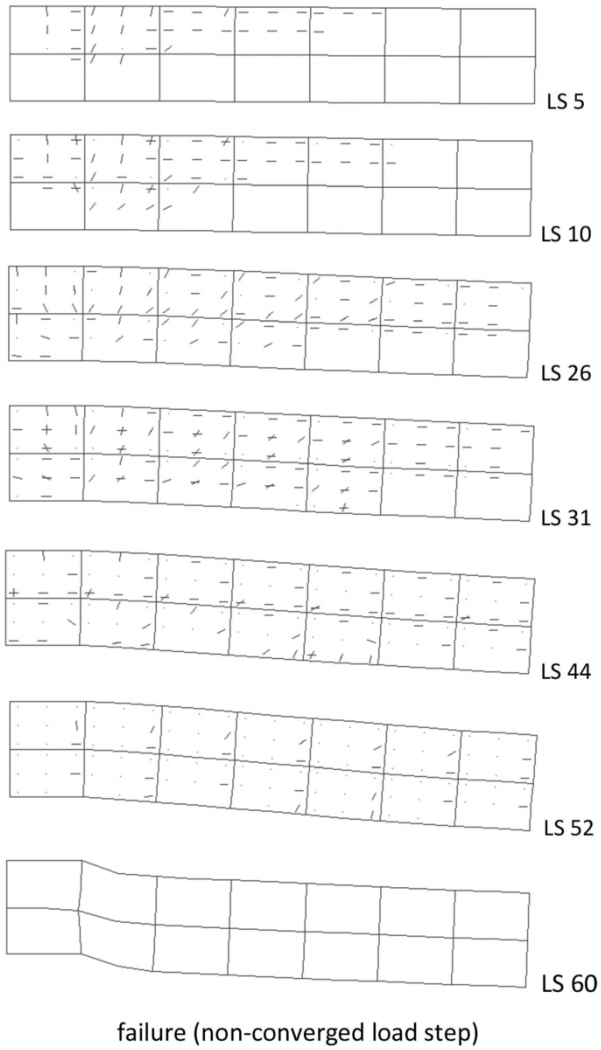

Fig. 13 Typical crack patterns at various load steps (LS) of slabs designed in compliance with EC2

From Table 3, it is also interesting to note that the load-carrying capacity of the specimens designed in accordance with the CFP method is similar to that of their counterparts designed in compliance with the EC2 code provisions when the target value of load-carrying capacity is not sufficient to cause yielding of the of the flexural tension reinforcement. Then, punching failure appears to be linked with the yielding of the transverse reinforcement bars along curve 1 indicated in Fig. 2. It should also be noted that, for all specimens in this case, the reinforcement arrangements for punching are similar to those in Figs. 6 to 8, but without the outer stirrup layer, whereas the amount of reinforcement is smaller by over 50% and uniformly distributed even for the case of the specimen designed in accordance with the CFP method.

From Tables 2 and 3, it can also be seen that, of the specimens designed in compliance with the EC2 requirements, those with the reinforcement for punching placed within the two strips extending along the *X* and *Y* axes of symmetry of the slab (see Fig. 7) exhibit a higher load-

Table 3 Variation of the load-carrying capacity of the specimens with $\rho_C=\rho_T$ with the method of design for a target load-carrying capacity equal to 760 kN

specimen	load-carrying capacity - kN		FEA/ des	EC2/ CFP	EC2-u/ EC2-s
	design	FEA			
T-CFP	760	711	0.9	-	-
T-EC2s		755	0.98	1.08	-
T-EC2u		655	0.86	0.95	0.88

Table 4 Variation of load-carrying capacity of the specimens under uniform displacement applied at a distance of 750 mm from the geometric centre of the slab along its diagonal and *X* and *Y* axes of symmetry.

specimen	load-carrying capacity - kN		FEA/ des	EC2/ CFP	EC2-u/ EC2-s
	design	FEA			
T-CFP	1500	1333	0.89	-	-
T-EC2s		980	0.65	0.73	-
T-EC2u		1005	0.67	0.75	1.03

carrying capacity than that of the specimens with reinforcement for punching uniformly distributed throughout the slab (see Fig. 8). The reason for such difference in behaviour appears to be linked with the locations where the load/displacement is applied. For the specimens investigated these locations essentially lie on the *X* and *Y* axes of symmetry of the slab, and, therefore, the applied load/displacement is primarily sustained by the slab strips extending between the load/displacement points on either side of the supporting column. Inducing the same displacements also at the points located on the slab's diagonal axes of symmetry at a distance from the geometric centre of the slab equal to that of the load/displacement points located on the *X* and *Y* axes of symmetry results in a more efficient distribution of the slab's resistance to the applied load/displacement, and, therefore, as indicated in Table 4, the uniformly distributed reinforcement for punching becomes more effective.

6. Conclusions

Numerical experiments are found to be an inexpensive and reliable means for assessing design tools such as the methods of design against punching failure that form the subject of the present work. The NLFEA package used for carrying out such experiments is shown to produce realistic predictions of structural behaviour which not only provide a close fit to data obtained from physical tests on the load-carrying capacity of slab-column sub-assemblages, but also an insight into the causes of punching failure.

In all cases investigated, the results obtained confirm those obtained in previous work which has demonstrated that, in contrast with current code adopted methods, the CFP method is capable of producing design solutions satisfying the current code requirements for structural performance. The reason for this has been found to be linked with the concepts underlying the development of the method which has been based on realistic considerations regarding the causes of punching. Unlike the CFP method, the method adopted by EC2 appears to ignore fundamental characteristics

of reinforced-concrete behaviour such as, for example, the development of transverse tensile stresses within the compressive zone linked with the loss of bond between concrete and tensile flexural reinforcement which has been found to be the cause of collapse of a number of flat-slab structures that occurred in recent years.

The results obtained are found to be independent of the presence and amount of compression flexural reinforcement. On the other hand, the locations of load points are found to have a small effect on the effectiveness of the design solutions obtained through the use of the code-adopted methods; the latter effect has been realistically predicted by the NLFEA package adopted for the work.

References

ADINA **(**2012), *Theory and Modelling Guide*, **1**.

Aoude, H., Cook, W.D. and Mitchell, D. (2013), "Two-way slab parking structures in Canada", *Concrete Product Guide*, 47.

Birkle, G. and Dilger, W.H. (2008), "Influence of slab thickness on punching shear strength", *ACI Struct. J.*, **105**(2), 180-188.

Eurocode 2 (2004), "Design of concrete structures-part 1-1: general rules and rules for buildings", EN 1992-1.

Hegger, J., Sherif, A.G. and Ricker, M. (2006), "Experimental investigations on punching behaviour of reinforced concrete footings", *ACI Struct. J.*, **103**(4), 604-613.

Kellermann, J.F. (1997), "Pipers row car park, wolverhampton: results of the investigation", *Concrete Car Parks: Design and Maintenance Issues*, Cavendish Centre, London, British Cement Association.

Kinnunen, S., Nylander, H. and Tolf, P. (1978), "Undersokningar rorande genemostansning vid Institutionen for Byggnadsstatik, KTH, *Nordisk Betong* (Stockholm), **3**, 25-27 (cited in Task Group 3.1/4.10, "Punching of structural concrete slabs", Technical report, Bulletin 12, fib (CEB-FIP).

Kotsovos, G.M. and Kotsovos, M.D. (2009), "Flat slabs without shear reinforcement: criteria for punching", *Struct. Eng.*, **87**(23/24), 32-38.

Kotsovos, G.M. and Kotsovos, M.D. (2010), "A new design method for punching of RC slabs: Verification by non-linear finite-element analysis", *Struct. Eng.*, **88**(8), 20-25.

Kotsovos, M.D. and Pavlovic, M.N. (1995), *Structural concrete: finite-element analysis for limit-state design*, Thomas Telford, London, Great Britain.

Kotsovos, M.D. (2014), *Compressive force-path method: unified ultimate limit-state design of concrete "Structures"*, Springer, London, UK.

Kotsovos, M.D. (2015), *Finite-element modelling of structural concrete: short-term static and dynamic loading conditions*, CRC Press (Taylor and Francis Group), Great Britain.

Morsch, E. (1902), "Versuche uber Schubspannungen in Betoneisentragen", *Beton und Eisen*, **2**(4), 269-274.

Mosley, B., Bungey, J. and Hulse, R. (2012), "Reinforced concrete design to Eurocode 2", 7th Edition, Palgrave Macmillan, UK.

Muttoni, A. (2008), "Punching shear strength of reinforced concrete slabs without transverse reinforcement", *ACI Struct. J.*, **105**(4), 440-450.

New Civil Engineer (1997), "Shock collapse sparks lift slab fears and Safety experts urge car park review", 27 March/3 April, 3-4.

Oliveira, D.R.C., Regan, P.E. and Melo, G.S.S.A. (2004), "Punching resistance of RC slabs with rectangularcolumns", *Mag. Concrete Res.*, **56**(3), 123-138.

Papanikolaou, K.V., Tegos, I.A. and Kappos, A.J. (2005), "Punching shear testing of reinforced concreteslabs and design implications", *Mag. Concrete Res.*, **57**(3), 167-177.

Ritter, W. (1899), "Die bauweise hennebique", *Schweisserische Bauzeitung*, **33**, 59-61.

Task Group 3.1/4.10 (2001), *Punching of structural concrete slabs*, Technical report, Bulletin 12, fib(CEB-FIP), April.

Yamada, T., Nanni, A. and Endo, K. (1993), "Punching shear resistance of flat slabs: Influence of reinforcement type and ratio", *ACI Struct. J.*, **88**(4), 555-563.

CC